Photoacoustics 13 (2019) 6–17

Contents lists available at ScienceDirect

Photoacoustics

journal homepage: www.elsevier.com/locate/pacs

Research article

A conjugated-polymer-based ratiometric nanoprobe for evaluating in-vivo hepatotoxicity induced by herbal medicine via MSOT imaging

Yinglong Wu[1], Lihe Sun[1], Fang Zeng*, Shuizhu Wu*

State Key Laboratory of Luminescent Materials and Devices, College of Materials Science and Engineering, South China University of Technology, Guangzhou, 510640, China

ARTICLE INFO

Keywords:
Optoacoustic imaging
Herbal medicine
Heptatoxicity
MSOT

ABSTRACT

Herbal medicines are widely used around the world, while some of them are associated with adverse effects like herb-induced liver injury due to oxidative/nitrosative stress resulted from hepatically-generated ROS/RNS. It is of significance to accurately evaluate herbal-medicine-induced hepatotoxicity, since it would help provide effective monitoring method of the safety of herbal remedies. Herein we designed a ratiometric nanoprobe for in vivo imaging hepatic injury induced by herbal medicine (polygonum multiflorum, PM) via specifically responding to NO generated in liver by PM, and with MSOT imaging the precise location of liver injury can be identified. The liposomal nanoprobe consists of a responsive dye (IX-2NH_2) which could specifically respond to NO and the diketopyrrolopyrrole-based conjugated polymer (DPP-TT) as the internal reference. Thus we can realize ratiometric optoacoustic detection of herbal-medicine-induced liver injury with 3D information in mouse model in a noninvasive way.

1. Introduction

Herbal medicine (botanical medicine) refers to using plants' roots, seeds, bark, leaves or flowers for medicinal purposes. As early as 3000 BCE ancient Chinese and Egyptian papyrus writings already described medicinal uses of plants [1,2]. Nowadays herbal medicines are still widely used around the world, especially in Asian countries. If used correctly, some herbs could help ameliorate or treat a variety of conditions [3]. But some herbs are toxic at high doses or if used improperly [4,5]; since herbal remedies usually consists of portions of plants or plant extracts which may have many constituents; and what specific ingredients can treat an illness or condition and which ones lead to the adverse effects are still not clearly known. The assumption that herbs are "natural" can be equated to "safe" is sometimes dangerously misleading, since some herbal medicines may contain pharmacologically active constituents which are associated with adverse effects ranging from gastrointestinal damage and allergic reactions to herbal hepatotoxicity or herb-induced liver injury [6–9], and the central role of the liver in metabolism assumably accounts for its susceptibility to drug-induced injury [10]. At present herbal medicinal products continue to grow and are often used as home remedies or over-the-counter drugs; but many of the herbal medicines remain untested and their use are often not properly monitored, and also the safety of many herbal products is further compromised by insufficient quality controls and the lack of adequate patient information [11]; whereas public health issues and concerns involving herbal medicines' safety have been increasingly recognized. Thus, it is of great significance to accurately detect and evaluate herbal-medicine-induced hepatotoxicity or liver injury, since it would help provide effective monitoring method of the safety of herbal remedies and ensure adequate protection of public health.

In medicine, biomarkers refer to quantifiable characteristics of some biological or disease states; they can be traceable substances like metabolites and enzymes [12]. As a noninvasive optical imaging method, fluorescent imaging technique has been adopted for detecting biomarker in terms of medical diagnosis or preclinical research [13–18]. Nonetheless, fluorescent detection method has limitations such as relatively low spatial resolution (diffuse-light-based imaging) and low penetration depth because of strong light scattering in deep tissue [19–21]. While optoacoustic (OA, also known as photoacoustic) imaging combines the good contrast and sensitivity attainable in optical imaging with the high resolution and deep penetration of ultrasound, and thus may avoid the shortcomings of conventional fluorescent imaging [22–30]. With pulsed-laser-light illumination (in in-vivo applications, longer NIR light wavelength would be beneficial, e.g. greater than 680 nm, because NIR light penetrates tissues more efficiently), because of light absorption, the probes undergo thermoelastic

* Corresponding authors.
E-mail addresses: mcfzeng@sc.edu.cn (F. Zeng), shzhwu@scut.edu.cn (S. Wu).
[1] These authors contributed equally to this work.

https://doi.org/10.1016/j.pacs.2018.11.002
Received 12 July 2018; Received in revised form 12 October 2018; Accepted 13 November 2018
Available online 16 November 2018

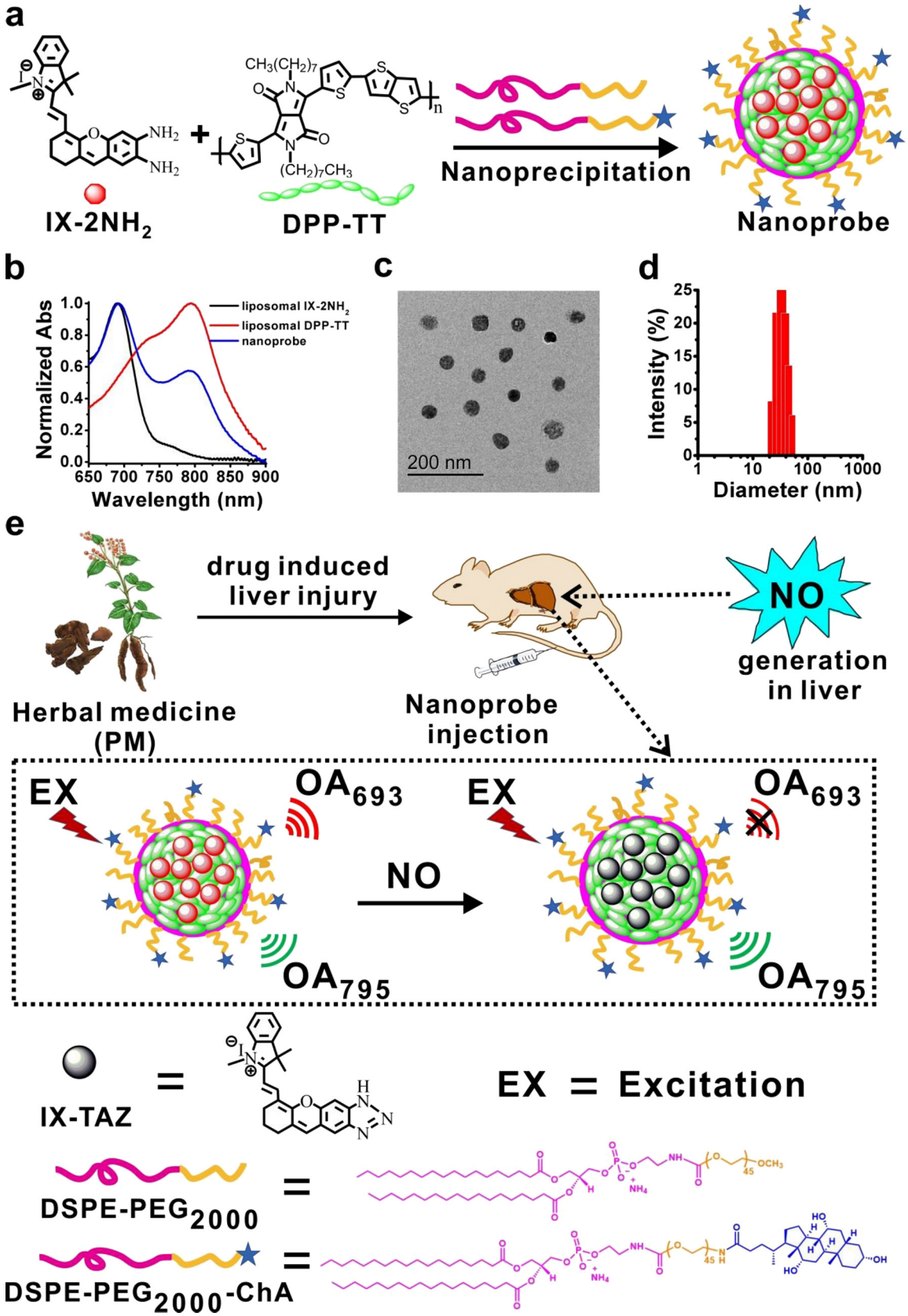

Fig. 1. Schematic illustration for the nanoprobe's detection of liver injury via responding to hepatic NO. (a) Formation of the nanoprobe consisting of the responsive dye IX-2NH_2 and the conjugated polymer DPP-TT. (b) Absorption spectra of the liposomal IX-2NH_2 nanoparticle, the liposomal DPP-TT nanoparticle and the nanoprobe. (c) TEM image of the nanoprobe. (d) Particle diameter distribution (DLS) for the nanoprobe. (e) Schematic presentation of herbal medicine (PM) induced NO upregulation in liver of mouse / subsequent liver injury and the nanoprobe's detection of liver injury via responding hepatic NO by MSOT imaging in a ratiometric way.

expansion and consequently generating ultrasound waves which are detected with ultrasound detector [31–33]. Hence, with OA imaging technique, noninvasive images of absorbed optical energy density in a region with the penetration depth up to several centimeters and a spatial resolution of around 100 μm can be obtained [31,32]. Optoacoustic tomography shows great potential for preclinical research and clinical practice [31,32]. More importantly, as the functional optoacoustic tomography, multispectral optoacoustic tomography (also known as MSOT) imaging technique is unaffected by photon scattering thus can providing high-resolution images deep inside biological tissues; and more importantly upon reconstruction from the collected 2D cross-sectional images, images with 3D information can be achieved [34–37], which is beneficial for precisely locating the focus of disease through detecting biomarkers with 3D information.

Currently hepatic toxicity of herbal medicines is usually detected via serum assay by measuring the significant elevation of some biomarker enzymes in serum including alanine aminotransferase (ALT), aspartate aminotransferase (AST) and alkaline phosphatase (ALP) as well as obvious liver histologic damage. However, many biomarkers are located in multiple organs or tissues besides the disease focus, which would erode the detection specificity of serum assay [38,39]. For example, the ALT enzyme is found in serum and multiple organ tissues especially liver, and significant concentrations are also found in kidney, skeletal muscle, and myocardium; lower levels of ALT are present in pancreas, spleen, and lung. The levels of serum ALT may be elevated in cases of liver or biliary duct damage, hepatitis, congestive heart failure or myopathy [38]. Hence, elevation in serum ALT does not necessary mean it is of hepatic origin. Whereas with MSOT imaging method, the elevation of the biomarker level at the specific organ (or tissue) can be spatially localized by using activatable optoacoustic probe, thereby greatly reducing the risks of false-positive signals.

Drug-induced liver injury often involves the intrinsic hepatotoxicity of the drug itself or, more frequently, the result of the toxic effects of its metabolites on vital cellular targets of liver. Drugs in the liver undergo enzymatic biotransformation which would generate reactive oxygen species (ROS) and reactive nitrogen species (RNS) [39]. The production of ROS and RNS (e.g. nitric oxide) accordingly results in intrahepatic oxidative/nitrosative stress, which contributes to initiation and progression of liver injury [39–41]. Thus ROS and RNS may act as alternative superior biomarker of drug-induced liver injury [41–43]. The ROS or RNS are short-lived and have half-lives typically of less than a second, which precludes their detection in serum and necessitates the in-situ detection at their sites of generation [43]. As the main components of some herbal medicines, anthraquinone and its derivatives are known to have the ability to oxidize glutathione (GSH) and thus depleting GSH significantly, which would result in oxidative stress and/or nitrosative stress through the overproduction of ROS and RNS and thereby lead to high hepatotoxicity [44,45]. Polygonum multiflorum (PM) is one of the most popular perennial Chinese herbal medicines, which has been officially listed in the Chinese Pharmacopoeia [46]. Its root tuber has been used as tonic and anti-aging agent (e.g. for treating premature gray hair and hair loss) [47,48]. However, PM mainly contains anthraquinone derivatives such as emodin and physcion, which have been found to induce heptatoxicity [49,50]. Therefore, ROS or RNS generated at the liver by herbal medicine like PM can be employed as a biomarker for detecting the herbal-medicine-induced liver injury (HILI).

In this study, we designed an optoacoustic nanoprobe for in vivo imaging hepatic injury induced by herbal medicine (PM) via specifically responding to the upregulated level of nitric oxide (NO) in liver induced by PM, and with MSOT imaging the precise location of liver injury can be identified. The liposomal nanoprobe consists of a near-infrared (NIR) dye (IX-2NH_2) as the responsive probe which could specifically respond to NO and the diketopyrrolopyrrole (DPP)-based conjugated polymer (DPP-TT) with NIR absorption as the internal reference. Furthermore, to afford the liver targeting capability for the nanoprobe, a bile acid modified and hepatocyte-targeting phospholipid DSPE-PEG2000-ChA was used. In the presence of NO, when the responsive dye (IX-2NH_2) reacts with NO, its NO-responsive unit diamino-containing xanthene turns into the triazole-containing xanthene and thereby generate the reaction product (IX-TAZ), accordingly the strong electron-donating diamino-containig xanethene group transforms into a weak electron-donating one (triazole-containig xanethene group), which correspondingly leads to the blue-shift of absorption and eventually lead to the significant changes in optoacoustic signaling. By using the optoacoustically-stable DPP-based conjugated polymer as the internal reference whose optoacoustic signal remains constant in physiological conditions, we can realize ratiometric optoacoustic detection of herbal-medicine-induced liver injury with 3D information in mouse model in a noninvasive way. The schematic illustration displaying the detection mechanism is shown in Fig. 1. And the experimental results indicate that, the nanoprobe can respond quickly to NO and provide 3D spatial information of herbal-medicine-induced liver injury.

2. Materials and methods

2.1. Preparation of the nanoprobe

First, the conjugated polymer DPP-TT (1 mg) was dissolved in THF (1 mL) by bath sonication and then filtered through a polyvinylidene fluoride (PVDF) syringe driven filter (0.22 μm) (Millipore). Then to the resultant solution, IX-2NH_2 (0.6 mg), DSPE-PEG_{2000} (2.0 mg) and DSPE-PEG_{2000}-ChA (0.5 mg) were successively added and dissolved. Afterwards, the above solution containing DPP-TT, IX-2NH_2 and DSPE-PEG_{2000} was rapidly injected into deoxygenized distilled-deionized water (9 mL) under continuous sonication for 5 min. After that, THF was evaporated at room temperature under reduced pressure. The aqueous solution was filtered through a polyethersulfone (PES) syringe driven filter (0.22 μm) (Millipore), and washed three times with water under centrifugation at 4000 rpm for 5 min at 4 °C. Finally, the nanoprobe were re-suspended in the phosphate buffer (or water for the concentration determination) and stored in dark at 2–8 °C. The liposomal IX-2NH_2 nanoparticles (the nanoparticles containing IX-2NH_2 alone and without DPP-TT) or liposomal DPP-TT nanoparticles (the nanoparticles containing DPP-TT alone and without IX-2NH_2) were also prepared with similar procedures and only without addition of DPP-TT or IX-2NH_2 respectively.

2.2. Mice model of INH-induced liver injury

All experiments involving animals were maintained under standard conditions and conducted in Laboratory Animal Center of South China Agricultural University; the experimental protocols have been approved by the Animal Ethics Committee of South China Agricultural University according to the guidelines for the care and use of laboratory animals. Male mice were divided into groups with six mice per group randomly, considering the sufficient replication of results and a reduction in animal number. Groups of male BALB/c nude mice (7 weeks old) were randomly selected for the following treatments. Animals were fasted for 8 h before all drug-induced hepatotoxicity imaging. Animals were injected intraperitoneally with sterilized saline solutions of isoniazid hydrazide (INH) (50, 100 or 200 mg/kg) for 3 h. The blood of the mice was collected for performing blood biochemical assay using ALP Elisa kits, and the livers were collected for histological analysis. Before dissection operation, the mice were euthanized humanly via being exposed to carbon dioxide in a rising concentration.

2.3. Mice model of herbal medicine induced liver injury

Male mice were divided into groups with six mice per group randomly. Groups of male BALB/c nude mice (7 weeks old) were selected randomly for the following treatments. Animals were subjected to oral

gavage administration of PM extract (the herbal crude drug (the roots of PM) was used to make the extract, with the dose of 18.5 g/kg (per kilogram of mouse body weight, in terms of herbal crude drug) once each day via oral gavage for continuous 1, 2 or 3 week(s). Animals were fasted for 8 h before imaging. Before dissection operation, the mice were euthanized humanly via being exposed to carbon dioxide in a rising concentration.

2.4. Optoacoustic tomography imaging

Optoacoustic imaging was conducted on an inVision128 multispectral optoacoustic tomographic (MSOT) imaging system (iThera Medical GmbH). As for phantom experiments, the test solution or the control (PBS) were filled fully in a commercial Wilmad NMR tube and were fixed respectively on the holder of the instrument. In vitro optoacoustic images of the nanoprobe in the presence of NO of varied concentrations were acquired (DPP-TT's signal at 795 nm and IX-$2NH_2$'s signal at 693 nm). As for in vivo optoacoustic imaging of drug-induced hepatotoxicity model, the mouse was anesthetized with 1% isoflurane which was delivered through a nose cone for the duration of the experiments. As for INH induced liver injury experiment, the mice were injected intravenously with liposomal IX-$2NH_2$ nanoparticles (IX-$2NH_2$ concentration 2.62 mg/kg). Similarly, the mice were intravenously injected with 23.6 mg/kg of the nanoprobe (which contains 2.62 mg/kg IX-$2NH_2$ and 3.1 mg/kg DPP-TT) for the herbal medicine-induced hepatotoxicity model. The mice were placed in the prone position in water bath at 34 °C, and the anaesthesia and oxygen were supplied via a breathing mask. The following imaging wavelengths were selected for being in correspondence with the absorption spectra of IX-$2NH_2$, DPP-TT and hemoglobin: 680 nm, 693 nm, 715 nm, 730 nm, 760 nm, 795 nm, 800 nm (used as background wavelength) and 850 nm. 10 individual frames were recorded for each wavelength. The in vivo optoacoustic images were acquired at 20 min after the nanoprobe injection by using the multispectral optoacoustic tomography system. A region of interest (ROI) volume consisting of transverse slices with a step size of 0.5 mm, which spans through the liver region, was chosen by manual inspection of live MSOT images. Guided ICA spectral unmixing in the imaging system was used to separate signals from IX-$2NH_2$, DPP-TT (no DPP-TT for INH-induced hepatotoxicity model) and those from the photo-absorbing tissue elements (e.g. hemoglobin). In in-vivo mouse optoacoustic imaging experiments, and for each group six mice were tested.

3. Results and discussions

3.1. Synthesis and fabrication of the nanoprobe

To construct the nanoprobe, first the responsive dye (IX-$2NH_2$) was synthesized by coupling the diamino-containing xanthene with indolium; while the conjugated polymer was synthesized via Stille coupling between 3,6-bis(5-bromo-2-thienyl)-2,5di-*n*-octylpyrrolo[3,4-c]pyrrole1,4-dione and 2,5-bis(trimethylstannyl)thieno[3,2-*b*]thiophene. The synthetic routes for the responsive dye (IX-$2NH_2$) as well as the conjugated polymer are shown in Scheme S1. The bile acid modified and hepatocyte-targeting phospholipid DSPE-PEG2000-ChA was prepared previously [51]. And the intermediate compounds and the responsive dye were characterized by ^{1}H NMR and mass spectrometry (MS) (Fig. S1-S6). The conjugated polymer was characterized by ^{1}H NMR; the molecular weight and its polydispersity of the conjugated polymer DPP-TT was measured by GPC (Fig. S7-S8). Afterwards the responsive dye and the conjugated polymer were encapsulated in phospholipid liposomes to enhance the solubility in blood, thus affording the nanoprobe. To ensure the liver-targeting capability of the nanoprobe, the cholic acid-modified phospholipid DSPE-PEG_{2000}-ChA (20 wt% in total lipids) was used together with DSPE-PEG_{2000} (80 wt% in total lipids) during the preparation of the nanoprobe. As for the nanoprobe, the contents of the responsive dye IX-$2NH_2$ and the conjugated polymer DPP-TT were determined as 11.1 wt% and 13.1 wt% respectively. Typical transmission electron microscopic (TEM) image and the diameter distribution determined by dynamic light scattering are shown in Fig. 1c and d respectively, it is clear that the average hydrodynamic diameter of the nanoprobe is about 42 nm, slightly larger than the size of the dried particles (around 40 nm).

3.2. Spectral properties and NO response of the responsive dye, the liposomal DPP-TT and the nanoprobe

First the spectral properties of the responsive dye were investigated. In the absence of NO, the responsive dye (IX-$2NH_2$) solution exhibited absorption at around 693 nm (Fig. S9b and Fig. 1b), and it also exhibited the highest optoacoustic signal at 693 nm (Fig. S9c); while in the presence of NO, after the dye's reaction with NO (the reaction product IX-TAZ) (Fig. S9a), the absorption blue-shifted to around 590 nm (Fig. S9b) and the absorption at 693 nm along with the OA signal at 693 nm decreased significantly (Fig. S9b and c). In the meantime, the fluorescence of the dye was also quenched in the presence of NO (Fig. S9d). Moreover, the responsive dye exhibited quite good selectivity toward NO (Fig. S9e). Thus the responsive dye can act as a turn-off detector for NO both optoacoustically and fluorescently. To confirm the dye's response mechanism toward NO, High Performance Liquid Chromatography (HPLC) was performed to analyze the reaction between NO and the dye. As displayed in Fig. S10a, as for the solution containing only the dye, the peak at 2.57 min that corresponds to the dye molecule could be observed. While upon the dye's reaction with NO, a new peak at 1.75 min appeared, which corresponds to the reaction product (IX-TAZ), and in the meantime the peak at 2.57 min decreased as the reaction time was increased; when the reaction was completed, the peak at 2.57 min disappeared, while that at 1.75 min further enhanced. In addition, the mass spectrum of the reaction mixture between the dye IX-$2NH_2$ and NO was also measured, as shown in Fig. S10b. Upon reaction between the dye and NO, in the reaction mixture the molecular weight peak at *m/z* 398.3 ($[M]^+$) corresponding to the probe molecule and the peak at *m/z* 409.2 ($[M]^+$) corresponding to the reaction product could be observed. These results demonstrate that, upon reaction with NO, the dye molecule transforms the diamino-containing dye (IX-$2NH_2$) to the triazole-contianing compound (IX-TAZ).

Next we measured the spectral properties of the liposomal conjugated polymer DPP-TT. It can be seen that liposomal DPP-TT exhibited an absorption band centering around 795 nm (Fig. S11), its OA signal also was the highest at 795 nm (Fig. S12a), and the polymer's OA signal showed a linear relationship to the polymer content (Fig. S12b). In the ratiometric OA nanoprobe, the role of the conjugated polymer is to act as the internal reference, which requires that it should have constant OA signal. Experimental results show that, the polymer displayed constant OA signal in the presence of various possible interfering species as well as in the wide range of pH values (Fig. S12c-d), which makes it a good candidate for serving as the internal reference.

And then the spectral properties of the nanoprobe were evaluated. In the absence of NO, the nanoprobe displayed two absorption bands centering at 693 nm and 795 nm respectively, which corresponded to the responsive dye and the conjugated polymer respectively (Figs. 2a and 1 b). In the presence of NO and as the NO level was increased or the reaction time was lengthened, the absorption at 693 nm decreased steadily, while that at 795 nm kept constant, indicating that the responsive dye IX-$2NH_2$ reacted with NO (Fig. 2a and Fig. S13). The absorption ratio (A_{795}/A_{693}) of the nanoprobe increased gradually as NO concentration or the reaction time was increased (Fig. 2b and Fig. S13), correspondingly the optoacoustic signal ratio (OA_{795}/OA_{693}) of the nanoprobe enhanced with the increasing NO level (Fig. 2d); the reaction between the nanoprobe and NO was completed within 4 min (Fig. S13); and the optoacoustic images of the nanoprobe in phantom at

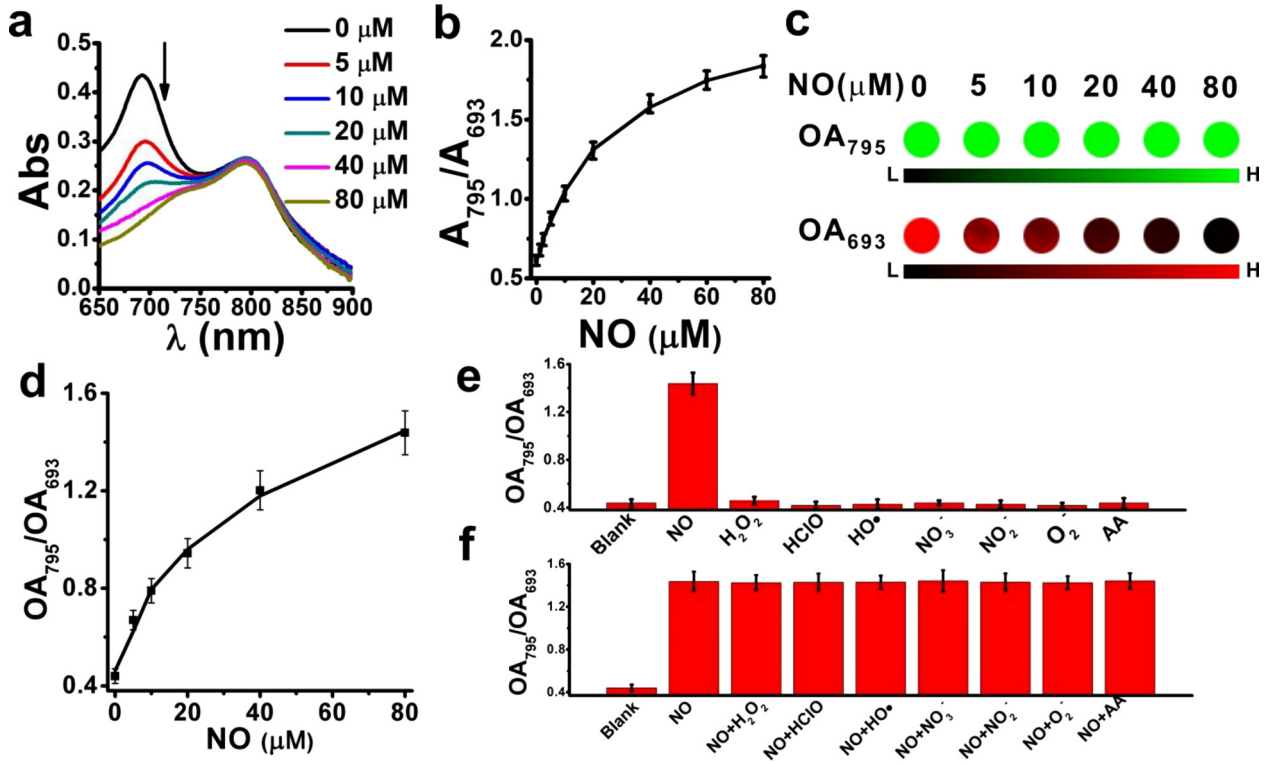

Fig. 2. (a) Absorption spectra of the nanoprobe (23.6 μg/mL) upon addition of NO with different concentrations for 4 min (DEA-NONOate was used as the NO donor). (b) Absorbance ratio (A_{795}/A_{693}) of the nanoprobe as a function of NO concentration. (c) Optoacoustic images of the nanoprobe in phantom with different NO concentrations (reaction time 4 min). (d). Optoacoustic signal ratio (O_{A795}/OA_{693}) of the nanoprobe as a function of NO concentration. (e) Optoacoustic response (optoacoustic signal ratio OA_{795}/OA_{693}) of the nanoprobe in the presence of 80 μM NO or a potential interference substance (80 μM of H_2O_2, HClO, HO·, NO^{3-}, NO^{2-}, O^{2-} or AA) (n = 3). (f) Optoacoustic response (optoacoustic signal ratio OA_{795}/OA_{693}) of the nanoprobe in the presence of 80 μM NO and simultaneously in the presence of a potential interference substance (80 μM of H_2O_2, HClO, HO·, NO^{3-}, NO^{2-}, O^{2-} or AA) (n = 3).

varied NO concentrations showed similar pattern (Fig. 2c). Furthermore, the nanoprobe exhibited specific response toward NO with quite good selectivity (Fig. 2e–f). These results establish that, the nanoprobe could serve as a good ratiometric detection system for in-vivo imaging of NO.

3.3. Cytotoxicities of IX-2NH2, liposomal DPP-TT and the nanoprobe, and IX-2NH2's response toward NO in living cells

The cytotoxicity measurements were carried out by using L929 cell line (which is known to have no expression of NO), HepG2 cell line and RAW264.7 cell line (which are known to have expression of NO) by MTT assay (in accordance with ISO 10993-5), and the results are displayed in Fig. S14a and Fig. S15. As for the responsive dye IX-$2NH_2$, it is clear that no obvious reduction in cell viabilities could be observed for all these cell lines treated with the dye even at the concentration of up to 50 μM, confirming that the responsive dye is suitable for live cell imaging. And also the conjugated polymer DPP-TT and the nanoprobe both exhibited little cytoxicities as well (Fig. S15).

As for L929 cells treated with the responsive dye, strong red fluorescence could be observed (Fig. S14b), because this cell line has no expression of NO. While for HepG2 and RAW264.7 cells, upon incubation with the responsive dye, red fluorescence was less strong than that in L929 cells (Fig. S14b). As for RAW264.7 cells upon stimulation with lipopolysaccharide (LPS), almost no red fluorescence could be observed due to the generation of NO upon LPS stimulation (Fig. S14b). However, when RAW264.7 cells were first treated with LPS and then with NO inhibitor PTIO, it can be seen that, the strong red fluorescence was restored in the cells (Fig. S14b). The results indicate that the fluorescence quenching in RAW264.7 cells is indeed triggered by the endogenously-generated NO.

3.4. Optoacoustic and fluorescent imaging of isoniazid-induced liver injury by liposomal IX-2NH2 nanoparticles

To confirm the responsive dye IX-$2NH_2$ can detect liver injury in vivo via responding to hepatic NO, it was evaluated experimentally by use of isoniazid-induced liver injury mice model which could cause hepatic NO increase. For this purpose and to ensure solubility in blood and liver-targeting capability, the responsive dye IX-$2NH_2$ was loaded into phospholipids (20 wt% of DSPE-PEG_{2000}-ChA and 80 wt% of DSPE-PEG_{2000}), thus affording the liposomal IX-$2NH_2$ nanoparticles. In order to determine the optimal time point for collecting optoacoustic data in the subsequent experiments, we first used optoacoustic imaging to evaluate the metabolism kinetics of the liposomal IX-$2NH_2$ nanoparticles. The liposomal IX-$2NH_2$ nanoparticles were intravenously injected into mice via tail vein, and then optoacoustic tomography imaging was performed; afterwards the cross-sectional images of the optoacoustic signal obtained via multispectral demixing were employed to evaluate the metabolism kinetics of the nanoparticles, and the results are shown in Fig. 3. As for the cross section corresponding to the liver region (namely that corresponding to the cryosection image of male mouse in Fig. 3i), upon i.v. injection of liposomal IX-$2NH_2$ nanoparticles, the OA signal of IX-$2NH_2$ increased gradually within 20 min (Fig. 3a), as can be seen from the mean signal intensity for the region of interest (ROI) as a function of time (Fig. 3b). After 25 min upon i.v. injection of the nanoparticles, the OA signal gradually decreased over time and the signal completely disappeared 24 h later (Fig. 3e–f). From this figure, the signal increased and decayed in the liver area can be clearly evaluated. This process actually involves two aspects: on one hand, upon i.v. injection the nanoparticles reached and accumulated in the liver through metabolism and generated OA signal upon excitation; on the other hand, the nanoparticles also underwent metabolic

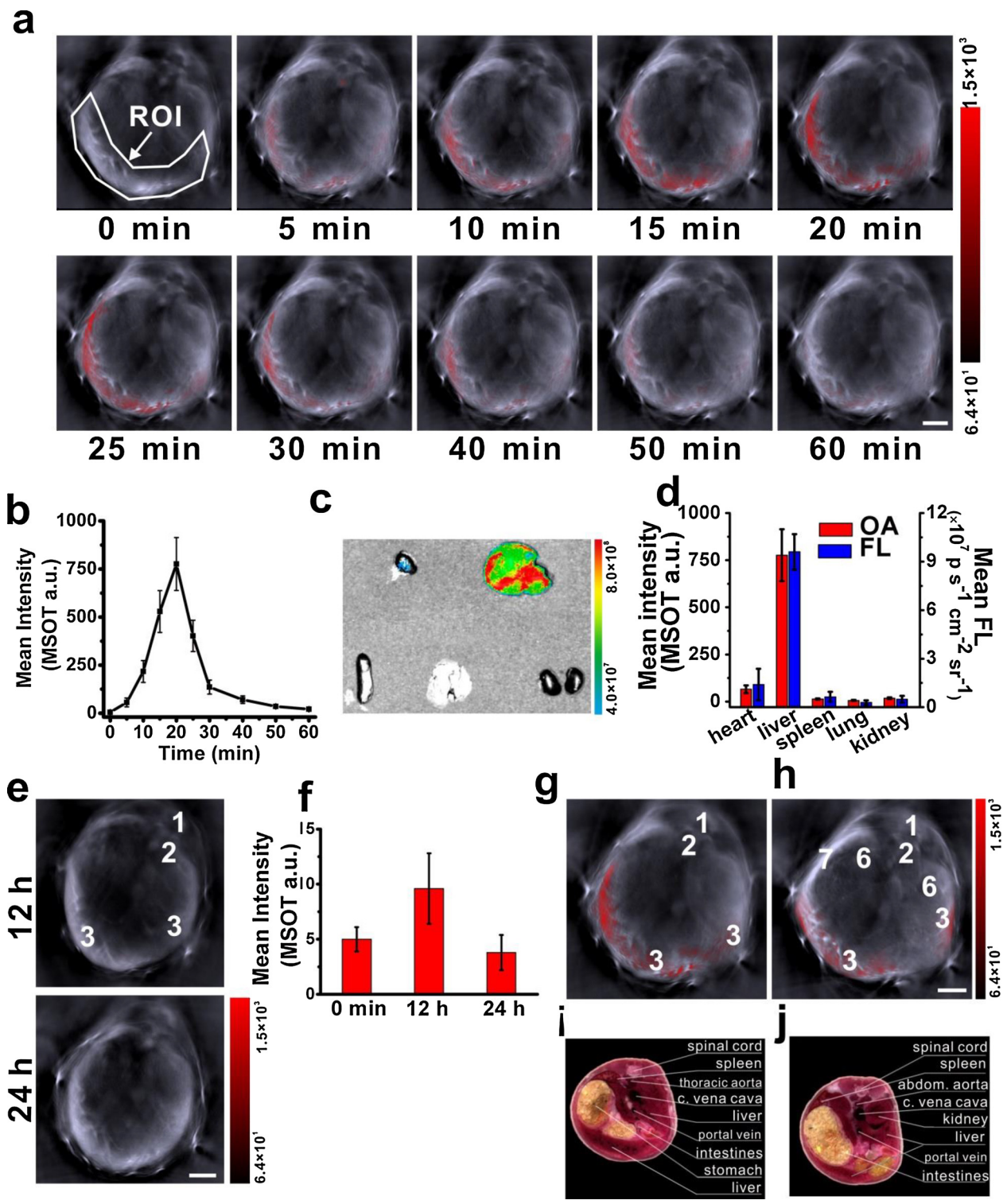

Fig. 3. Metabolism kinetics of liposomal IX-2NH_2 nanoparticles. (a) Representative cross sectional MSOT images of the mouse upon i.v. injection of liposomal IX-2NH_2 nanoparticles. (b) OA signal intensity as a function of time (corresponding to the images in a). (c) Representative fluorescence images for the excised main organs of the mouse at 20 min after i.v. injection of liposomal IX-2NH_2 nanoparticles (top row from left to right: heart, liver; bottom row from left to right: spleen, lung, kidney). (d) Optoacoustic signal and fluorescent signal intensity of the excised main organs of the mouse at 20 min after i.v. injection of liposomal IX-2NH_2 nanoparticles. (e) Representative cross sectional MSOT images of the mouse upon i.v. injection of liposomal IX-2NH_2 nanoparticles. (f) OA signal intensity as a function of time (0 min corresponding to the images in a; 12 h and 24 h corresponding to the images in e). (g) and (h) Different cross sectional MSOT images recorded at 20 min after i.v. injection of liposomal IX-2NH_2 nanoparticles. (1: spinal cord, 2: aorta, 3: liver, 6: kidney, 7: spleen). (i) and (j) cryosection image of a male mouse (corresponding to those in g and h respectively).

clearance from the liver. The results indicate that, 20 min would be the time when most of the nanoparticles reached the liver right before the beginning of obvious clearance; hence in subsequent experiments 20 min (after injection of the detection systems) was chosen as the time point for measuring optoacoustic or fluorescent signals for detecting liver injury. Although the intrinsic hepatic NO in healthy mice (at low concentration) would react with IX-2NH_2 during the whole metabolic process; for facilitating analysis, this minor effect was ignored in the following in-vivo imaging experiments. In addition, at 20 min after i.v. injection of liposomal IX-2NH_2 nanoparticles, the fluorescence images for the excised main organs of the mouse were also recorded (Fig. 3c), these images indicate that only the liver exhibited strong fluorescence. Both the optoacoustic and fluorescent signal intensities for the major organs at 20 min after i.v. injection of liposomal IX-2NH_2 nanoparticles also showed that only the liver had strong signal (Fig. 3d), indicating the liposomal IX-2NH_2 nanoparticles mainly reside in the liver probably due to the existence of the liver-targeting DSPE-PEG_{2000}-ChA. Moreover, the images at different cross sections for the mice injected with the liposomal IX-2NH_2 nanoparticles are displayed in Fig. 3g–h to reflect the OA signal intensities at different cross sections and the corresponding cryosection images of mouse are shown in Fig. 3i–j; from these images it is clear only the liver region displayed strong OA signal, the result again confirmed that the nanoparticles mainly resided in the liver.

On the basis of the above experimental results, isoniazid (isonicotinyl hydrazide, referred to as INH) which is an antibiotic clinically used for the treatment of tuberculosis, was used to induce liver injury in mice for evaluating liposomal IX-2NH_2's capability of detecting the changes of hepatic NO. Isoniazid is known to be metabolized by hepatic N-acetyltransferase and cytochrome P450 to increase hepatic NO and further produce hepatotoxins, thereby leading to liver injury and even hepatitis [52–54]. Isoniazid was administered intraperitoneally to male nude mice, followed by i.v. injection of liposomal IX-2NH_2 nanoparticles. As shown in Fig. 4, upon the treatment of isoniazid with different doses [43,55,56], and as the dosage is increased, the OA signal of IX-2NH_2 in the liver region steadily decreases (Fig. 4a-b), which indicates that treating a mouse with higher isoniazid dose would cause more severe liver damage; MSOT images with 3D information also clearly showed similar pattern (Fig. 4g and Fig. S16); and these results indicate that the responsive dye IX-2NH_2 acts as a turn-off optoacoustic probe for detecting liver damage via responding to hepatic NO. The fluorescent imaging for the mice upon isoniazid treatment was also conducted. It can be seen that, upon isoniazid treatment the mice exhibits decreasing fluorescent signal at abdominal area, as the isoniazid dosage is increased (Fig. 4c-d). The serum ALP level of the mice increased as the drug dosage is increased (Fig. 4e), which confirms the increasing severity of liver injury. Moreover, histological studies of the liver's tissue sections were conducted through H&E staining, as shown in Fig. 4f and Fig. S17; histological examination of the stained liver tissue indicates obvious liver damages induced by the drug isoniazid.

3.5. The nanoprobe's in-vivo toxicity and MSOT images with 3D information of herbal-medicine-induced liver injury in mouse model

Compared with the turn-on mode imaging, ratiometric optoacoustic imaging involves the simultaneous measurement of two optoacoustic signals followed by calculation of their intensity ratio, and a few ratiometric nanoprobes for optoacoustic imaging have been developed for realizing more precise analysis [57–63]. Based on the above experimental results, it is clear that the responsive dye IX-2NH_2 could serve as a selective turn-off probe for detecting hepatic NO level in vivo thereby imaging drug-induced liver damage, and the liposomal nanoparticles made with the liver-targeting phospholipid (DSPE-PEG_{2000}-ChA) can efficaciously target the liver, which pave the way for using the nanoprobe to ratiometrically detect liver injury induced by herbal medicine (PM). Before employing the nanoprobe for ratiometrically detect herbal-medicine-induced liver injury via MSOT imaging, we first assessed the in-vivo toxicity of the nanoprobe by conducting serum biochemistry and organ histology as well as measuring the body weight of mouse. From Fig. S18, it is clear that no significant differences in the body weight could be observed for different mice groups, namely the control group (healthy mice) and the treatment groups that were intravenously injected with the nanoprobe or liposomal IX-2NH_2 nanoparticles. As for serum biochemistry, the measured parameters include the representative parameters such as total bilirubin (TBIL), alanine aminotransferase (ALT) and aspartate aminotransferase (AST) that reflect the liver function, as well as those reflecting kidney function including creatinine (CREA), serum urea (UREA) and blood urea nitrogen (BUN); and the results are shown in Fig. S19. For the control group and the treatment groups, these serum parameters are quite similar, confirming that the nanoprobe's in-vivo toxicity is insignificant. Furthermore, histological studies were conducted via H&E staining for the tissue sections of the major organs (heart, liver, lung, spleen and kidney) of the control group (healthy mice) and the treatment groups i.v. injected with the nanoprobe or liposomal IX-2NH_2 nanoparticles; and the results are displayed in Fig. S20. Clearly no obvious histopathological abnormalities can be observed among the three groups; these results again confirm that the nanoprobe has little in-vivo toxicity.

Next, polygonum multiflorum (PM), whose roots has been a popular herbal remedy for anti-aging and low libido and which is known for possible hepatotoxicity, was utilized to induce liver injury in this study. As for therapeutic drugs, the dose conversion or translation from animal to human or vice versa can be made [64–69]. The herbal crude drug are the from PM's roots, and the dried powder from extracts of herbal crude drug was dispersed in 0.5% carboxymethyl cellulose sodium salt aqueous solution for oral gavage administration; the dosage of 18.5 g/kg (in terms of herbal crude drug) was used in the mouse model in this study, and was administered via oral gavage in mice every day for 7, 14 or 21 days. This dose is equivalent to 15 times of the upper dose for human stipulated in Chinese Pharmacopoeia [46,64,65]. Then the multispectral optoacoustic tomography (also known as MSOT) imaging technique was used to detect the herbal-medicine-induced liver injury (HILI) through imaging the changes of hepatic NO; and the results are shown in Figs. 5 and 6. The cross-sectional images reconstructed from the MSOT signals from the mice for different treatment time (herbal medicine treatment) were obtained at 20 min after the nanoprobe was injected intraveneously via tail vein. By multispectral demixing, the MSOT images include: the background image (as an anatomical reference); the overlay of the conjugated polymer's (DPP-TT) image with the background; the overlay of the IX-2NH_2's image with the background; and the superposition of the DPP-TT's image, the IX-2NH_2's image and the background. As for the control group of mice which were not treated with the herbal medicine, 20 min upon injection of the nanoprobe, strong signals from DPP-TT and IX-2NH_2 could be observed. As for the mice groups that were treated with herbal medicine, as the treatment time increased from one week to three weeks, the DPP-TT's OA signal kept constant; while the IX-2NH_2's signal almost remained strong for the groups with the treatment time of one week, but for the group with the treatment time of two or three weeks IX-2NH_2's signal decreased steadily. The results indicate that, as the treatment time is lengthened, hepatic NO increased and liver injury is caused by the herbal medicine for the relatively long term of treatment (Fig. 5a–b). Through referring to a cryosection image of a male mouse (Fig. 3i), it is clear that the OA signals of both DPP-TT and IX-2NH_2 are in the liver area. The mice' serum ALP level also increased as the treatment time was lengthened (Fig. 5c). And histological studies of the liver tissue sections confirm that, for the treatment time of one week, no liver damage can be observed; and slight liver damage can only be observed in the mice with the treatment time of two weeks; while significant liver damage is clear with the treatment time of three weeks (Fig. 5d).

The MSOT images with 3D information for the mice groups with or

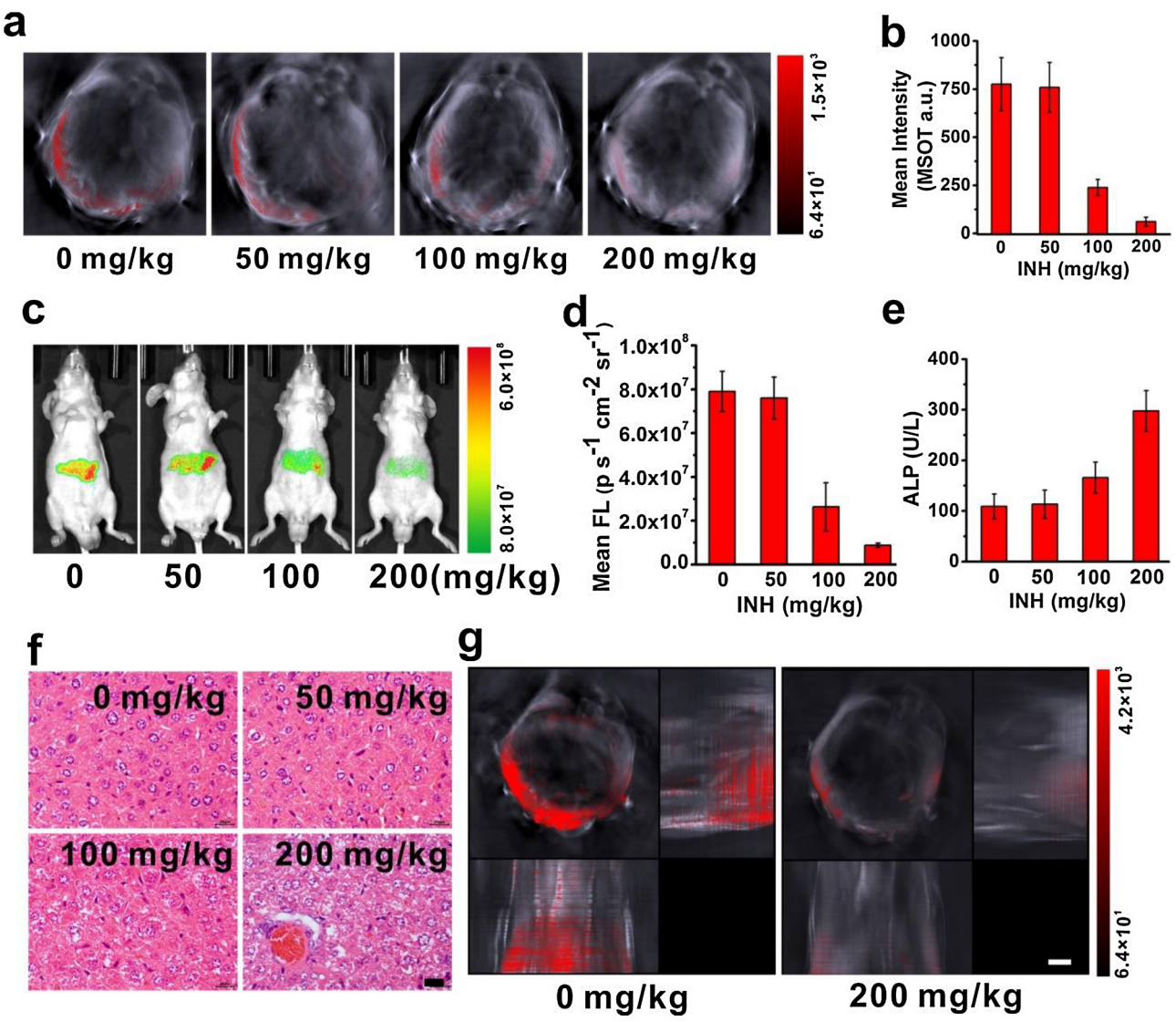

Fig. 4. Optoacoustic imaging of INH-induced liver injury by liposomal IX-2NH$_2$ nanoparticles. (a) Representative cross sectional MSOT images of the mouse treated with different doses of INH for 3 h, and the images were recorded at 20 min after the injection of liposomal IX-2NH$_2$ nanoparticles. (b) OA signal intensity as a function of INH dosage (corresponding to the images in a). (c) Representative fluorescence images of the mice treated with different doses of INH for 3 h, and the images were recorded at 20 min after the injection of liposomal IX-2NH$_2$ nanoparticles. (d) Fluorescence signal intensity as a function of INH dosage (corresponding to the images in c). (e) Serum ALP level as a function of INH dosage for the mice treated with different doses of INH for 3 h. (f) Representative histological sections (H &E staining) for main organs of the mice treated with different INH dosage. (g) Representative MSOT images (orthogonal views) with 3D information for the control and the mice treated with 200 mg/kg of INH for 3 h, and the images were recorded at 20 min after injection of liposomal IX-2NH$_2$ nanoparticles.

without herbal-medicine treatment are shown in Fig. 6. The images were obtained from multiple cross-sectional slices via using the ViewMSOT software supplied with the system; and these images with 3D information allow for the volumetric visualization of specific signals inside the mice. As for the control group (the mice that did not undergo herbal medicine treatment) (Fig. 6a), the OA signals of both the DPP-TT and IX-2NH$_2$ are very strong, indicating there was no liver injury since heptatic NO didn't increase. As for the mice that underwent treatment with the herbal medicine for three weeks (Fig. 6b), the signal of DPP-TT remained constant, while that of IX-2NH$_2$ decreased significantly, indicating obvious liver damage has been caused. The injured liver can be visualized clearly, and it can be seen that the volume of the injured liver is quite large. In addition, the response of the nanoprobe towards the herbal-medicine treatment for three weeks is shown in Fig. 6b, which indicates that treating a mouse with the herbal medicine for a relatively long period (three weeks) would cause liver damage. Moreover, histological analysis of liver sections from the mice before and after herbal-medicine treatment (Fig. 5d and Fig. S21) offers further evidence that, the herbal-medicine-treated mice upon three weeks' treatment suffered obvious hepatic injury. Altogether the results indicate that, the elevated hepatic NO as a result of liver injury induced by herbal medicine can be detected by MSOT imaging in a temporal and spatial manner.

In summary, for the first time we have successfully developed the ratiometric optoacoustic nanoprobe for imaging herbal-medicine induced liver injury via detection of hepatic NO. Moreover, with MSOT imaging and by using the nanoprobe, the precise location of liver injury can be identified in real time. We suppose this strategy may serve as a promising approach for evaluating adverse effects related to herbal-medicine treatments via detecting variations of other biomarkers in vivo, as well as for monitoring the safety of herbal medicine.

Conflict of interest

The authors declare no conflict of interest.

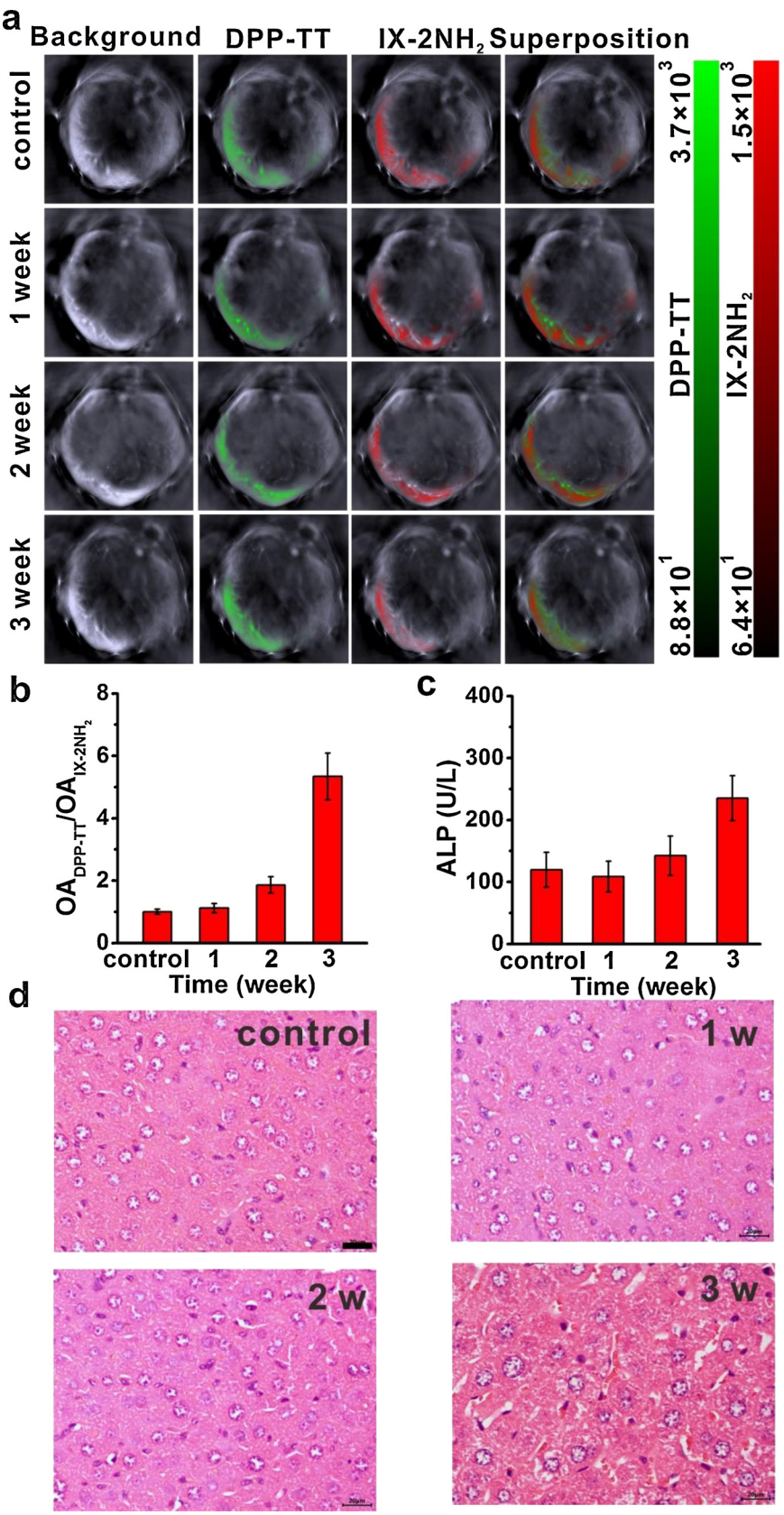

Fig. 5. (a) Representative cross sectional MSOT images of the control and the mice treated by herbal medicine for different time, and the images were recorded at 20 min after injection of the nanoprobe. (b) OA signal ratio as a function of treatment time (corresponding to the images in a), $OA_{DPP\text{-}TT}/OA_{IX\text{-}2NH2}$ = $[(OA_{DPP\text{-}TT})_{time}$ / $(OA_{DPP\text{-}TT})_{control}]$ / $[(OA_{IX\text{-}2NH2})_{time}$ / $(OA_{IX\text{-}2NH2})_{control}]$. (c) Serum ALP levels of the control and the mice treated with herbal medicine for different time. (d) Representative histological sections (H&E staining) for the liver of the mice treated with the herbal medicine for different time (scale bar: 20 μm).

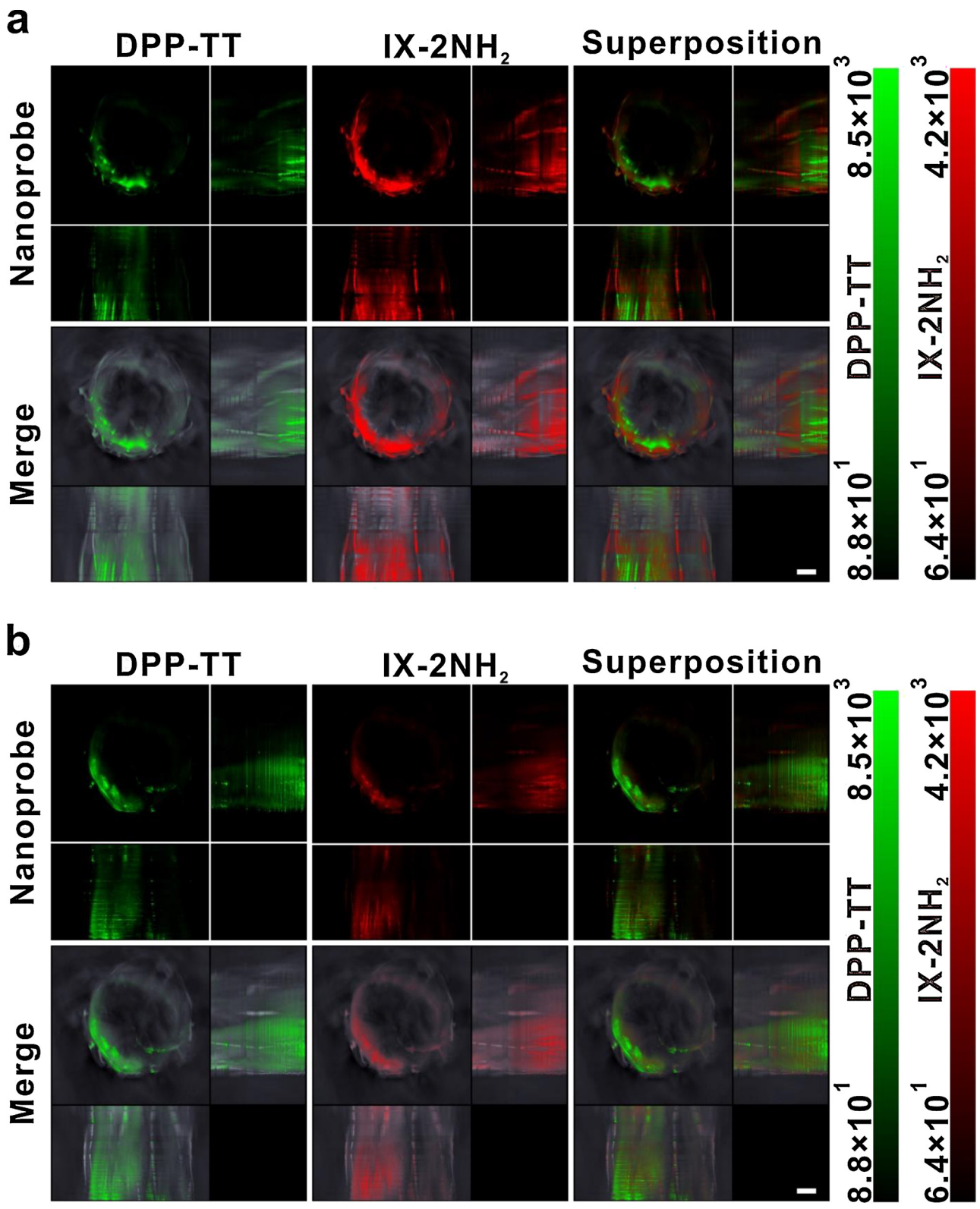

Fig. 6. MSOT images (orthogonal views) with 3D information. (a) Representative MSOT images of the control mice group. (b) Representative MSOT images the mice group treated with herbal medicine for three weeks. The images were recorded at 20 min after the injection of the nanoprobe.

Acknowledgments

This work was supported by NSFC (21875069, 51673066, 21574044, and 21474031), the Science and Technology Planning Project of Guangzhou (Project No. 201607020015), the Natural Science Foundation of Guangdong Province (2016A030312002).

Appendix A. Supplementary data

Supplementary material related to this article can be found, in the

online version, at doi:https://doi.org/10.1016/j.pacs.2018.11.002.

References

[1] L. Liu, C. Liu, Y. Wang, P. Wang, Y. Li, B. Li, Herbal medicine for anxiety, depression and insomnia, Curr. Neuropharmacol. 13 (2015) 481–493.
[2] F.S. Li, J.K. Weng, Demystifying traditional herbal medicine with modern approach, Nat. Plants 3 (2017) 17109.
[3] W. Lam, S. Bussom, F. Guan, Z. Jiang, W. Zhang, E.A. Gullen, S.H. Liu, Y.C. Cheng, The four-herb chinese medicine PHY906 reduces chemotherapy-induced gastrointestinal toxicity, Sci. Transl. Med. 2 (2010) 45ra59.
[4] M. Ekor, The growing use of herbal medicines: issues relating to adverse reactions and challenges in monitoring safety, Front. Pharmacol. 4 (2013) 177.
[5] J.L. Nortier, M.M. Martinez, H.H. Schmeiser, V.M. Arlt, C.A. Bieler, M. Peterin, M.F. Depierreux, L. De Pauw, D. Abramowicz, P. Vereerstraeten, J.L. Vanherweghem, Urothelial Carcinoma Associated with the Use of a Chinese Herb (Aristolochia fangchi), N. Engl. J. Med. 342 (2000) 1686–1692.
[6] B. Niggemann, C. Gruber, Side-effects of complementary and alternative medicine, Allergy 58 (2003) 707–716.
[7] P. Posadzki, L.K. Watson, E. Ernst, Adverse effects of herbal medicines: an overview of systematic reviews, Clin. Med. 13 (2013) 7–12.
[8] R. Teschke, C. Frenzel, X. Glass, J. Schulze, A. Eickhoff, Herbal Hepatoxicity: A Critical Review, Br. J. Clin. Pharmacol. 75 (2012) 630–636.
[9] A. Fugh-Berman, Herb-drug interactions, Lancet 355 (2000) 134–138.
[10] A. Corsini, M. Bortolini, Drug-induced liver injury: the role of drug metabolism and transport, J. Clin. Pharmacol. 53 (2013) 463–474.
[11] D.K. Raynor, R. Dickinson, P. Knapp, A.F. Long, D.J. Nicolson, Buyer beware? Does the information provided with herbal products available over the counter enable safe use? BMC Med. 9 (2011) 94.
[12] J. Aronson, Biomarkers and surrogate endpoints, British J. Clin. Pharmacol. 59 (2005) 491–494.
[13] G. Lin, P.N. Manghnani, D. Mao, C. The, Y. Li, Z. Zhao, B. Liu, B.Z. Tang, Robust red organic nanoparticles for in vivo fluorescence imaging of cancer cell progression in xenografted zebrafish, Adv. Funct. Mater. 27 (2017) 1701418.
[14] K. Gu, Y. Xu, H. Li, Z.Q. Guo, S.J. Zhu, S.Q. Zhu, P. Shi, T.D. James, H. Tian, W.H. Zhu, Real-time tracking and in vivo visualization of β-galactosidase activity in colorectal tumor with a ratiometric near-infrared fluorescent probe, J. Am. Chem. Soc. 138 (2016) 5334–5340.
[15] B. Li, X. Xie, Z. Chen, C. Zhan, F. Zeng, S. Wu, Tumor inhibition achieved by targeting and regulating multiple key elements in egfr signaling pathway using a self-assembled nanoprodrug, Adv. Funct. Mater. 28 (2018) 1800692.
[16] H.Y. Huang, J.F. Lovell, Advanced functional nanomaterials for theranostics, Adv. Funct. Mater. 27 (2017) 1603524.
[17] Y. Wu, J. Wang, F. Zeng, S. Huang, J. Huang, H. Xie, C. Yu, S.Z. Wu, Pyrene derivative emitting red or near-infrared light with monomer/excimer conversion and its application to ratiometric detection of hypochlorite, ACS Appl. Mater. Interfaces 8 (2016) 1511–1519.
[18] Z. Wang, H. Wu, P. Liu, F. Zeng, S. Wu, A self-immolative prodrug nanosystem capable of releasing a drug and a NIR reporter for in vivo imaging and therapy, Biomaterials 139 (2017) 139–150.
[19] B. Li, P. Liu, H. Wu, X. Xie, Z. Chen, F. Zeng, S. Wu, A bioorthogonal nanosystem for imaging and in vivo tumor inhibition, Biomaterials 138 (2017) 57–68.
[20] Y. Huang, P. Zhang, M. Gao, F. Zeng, A. Qin, S. Wu, B.Z. Tang, Ratiometric detection and imaging of endogenous hypochlorite in live cells and in vivo achieved by using an aggregation induced emission (AIE)-based nanoprobe, Chem. Commun. 52 (2016) 7288–7291.
[21] C. Yu, X. Li, F. Zeng, F. Zheng, S.Z. Wu, Carbon-dot-based ratiometric fluorescent sensor for detecting hydrogen sulfide in aqueous media and inside live cells, Chem. Commun. 49 (2013) 403–405.
[22] R. Nagaoka, T. Tabata, S. Yoshizawa, S.I. Umemura, Y. Saijo, Visualization of murine lymph vessels using photoacoustic imaging with contrast agents, Photoacoustics 9 (2018) 39–48.
[23] A.P. Jathoul, J. Laufer, O. Ogunlade, B. Treeby, B. Cox, E. Zhang, P. Johnson, A.R. Pizzey, B. Philip, T. Marafioti, M.F. Lythgoe, R.B. Pedley, M.A. Martin, P. Beard, Deep in vivo photoacoustic imaging of mammalian tissues using a tyrosinase-based genetic reporter, Nature. Photon. 9 (2015) 239–246.
[24] A.R. Mohammadi-Nejad, M. Mahmoudzadeh, M.S. Hassanpour, F. Wallois, O. Muzik, C. Papadelis, A. Hansen, H. Soltanian-Zadeh, J. Gelovani, M. Nasiriavanaki, Neonatal brain resting-state functional connectivity imaging modalities, Photoacoustics 10 (2018) 1–19.
[25] M.T. Berninger, P. Mohajerani, M. Wildgruber, N. Beziere, M.A. Kimm, X. Ma, B. Haller, M.J. Fleming, S. Vogt, M. Anton, A.B. Imhoff, V. Ntziachristos, R. Meier, T.D. Henning, Detection of intramyocardially injected DiR-labeled mesenchymal stem cells by optical and optoacoustic tomography, Photoacoustics 6 (2017) 37–47.
[26] R. Ni, M. Rudin, J. Klohs, Cortical hypoperfusion and reduced cerebral metabolic rate of oxygen in the arcAbeta mouse model of Alzheimer's disease, Photoacoustics 10 (2018) 38–47.
[27] A. Shah, N. Bush, G. Box, S. Eccles, J. Bamber, Value of combining dynamic contrast enhanced ultrasound and optoacoustic tomography for hypoxia imaging, Photoacoustics 8 (2017) 15–27.
[28] M.J. Duffy, O. Planas, A. Faust, T. Vogl, S. Hermann, M. Schafers, S. Nonell, C.A. Strassert, Towards optimized naphthalocyanines as sonochromes for photoacoustic imaging in vivo, Photoacoustics 9 (2018) 49–61.
[29] Y. Cao, A. Kole, L. Lan, P. Wang, J. Hui, M. Sturek, J.X. Cheng, Spectral analysis assisted photoacoustic imaging for lipid composition differentiation, Photoacoustics 7 (2017) 12–19.
[30] K. Haedicke, C. Brand, M. Omar, V. Ntziachristos, T. Reiner, J. Grimm, Sonophore labeled RGD: a targeted contrast agent for optoacoustic imaging, Photoacoustics 6 (2017) 1–8.
[31] L.V. Wang, S. Hu, Photoacoustic tomography: in vivo imaging from organelles to organs, Science 335 (2012) 1458–1462.
[32] L.V. Wang, J. Yao, A practical guide to photoacoustic tomography in the life sciences, Nat. Methods 13 (2016) 627–638.
[33] A.B.E. Attia, S.Y. Chuah, D. Razansky, C.J.H. Ho, P. Malempati, U.S. Dinish, R. Bi, C.Y. Fu, S.J. Ford, J.S.S. Lee, Noninvasive real-time characterization of non-melanoma skin cancers with handheld optoacoustic probes, Photoacoustics 7 (2017) 20–26.
[34] D. Razansky, A. Buehler, V. Ntziachristos, Volumetric real-time multispectral optoacoustic tomography of biomarkers, Nat. Protoc. 6 (2011) 1121–1129.
[35] S. Tzoumas, N.C. Deliolanis, S. Morscher, V. Ntziachristos, Unmixing molecular agents from absorbing tissue in multispectral optoacoustic tomography, IEEE Trans. Med. Imaging 33 (2014) 48–60.
[36] S. Tzoumas, A. Kravtsiv, Y. Gao, A. Buehler, V. Ntziachristos, Statistical molecular target detection framework for multispectral optoacoustic tomography, IEEE Trans. Med. Imaging 35 (2016) 2534–2545.
[37] D. Razansky, J. Baeten, V. Ntziachristos, Sensitivity of molecular target detection by multispectral optoacoustic tomography (MSOT), Med. Phys. 36 (2009) 939–945.
[38] M.A. Suckow, K.A. Stevens, R.P. Wilson (Eds.), The Laboratory Rabbit, Guinea Pig, Hamster, and Other Rodents, Elsevier, New York, 2012.
[39] V.B. Patel, R. Rajendram, V.R. Preedy (Eds.), The Liver: Oxidative Stress and Dietary Antioxidants, Academic press / Elsevier, Landon, 2018.
[40] I.S. Evan, M.E. Sahar, O.S. Mabrouka, E.B. Azza, Role of oxidative stress and nitric oxide in the protective effects of a-lipoic acid and aminoguanidine against isoniazid-rifampicin induced hepatotoxicity in rats, Food Chem. Toxicol. 48 (2010) 1869–1875.
[41] D.J. Antoine, D.P. Williams, B.K. Park, Understanding the role of reactive metabolites in drug-induced hepatotoxicity: state of the science, Expert Opin. Drug Metab. Toxicol. 4 (2008) 1415–1427.
[42] S. Russmann, G.A. Kullak-Ublick, I. Grattagliano, Curr. Med. Chem. 16 (2009) 3041–3053.
[43] A. Shuhendler, K.Y. Pu, L. Cui, J.P. Uetrecht, J.H. Rao, Real-time imaging of oxidative and nitrosative stress in the liver of live animals for drug-toxicity testing, Nat. Biotech. 32 (2014) 373–380.
[44] J. Yi, J. Yang, R. He, F. Gao, H. Sang, X. Tang, R.D. Ye, Emodin enhances arsenic trioxide-induced apoptosis via generation of reactive oxygen species and inhibition of survival signaling, Cancer Res. 64 (2004) 108–116.
[45] L. Salmon-Chemin, E. Buisine, V. Yardley, S. Kohler, M. Debreu, V. Landry, C. Sergheraert, S.L. Croft, R.L. Krauth-Siegel, E. Davioud-Charver, 2- and 3-Substituted 1,4-naphthoquinone derivatives as subversive substrates of trypanothione reductase and lipoamide dehydrogenase from trypanosoma cruzi: synthesis and correlation between redox cycling activities and in vitro cytotoxicity, J. Med. Chem. 44 (2001) 548–565.
[46] Pharmacopoeia of the People's Republic of China, Chinese Pharmacopoeia Commission, 2015, pp 175-177.
[47] J.N. Grech, Q. Li, B.D. Roufogalis, C.C. Duck, Novel Ca^{2+}-ATPase inhibitors from the dried root tubers of polygonum multiflorum, J. Nat. Prod. 57 (1994) 1682–1687.
[48] D. Gao, J. Pang, C. Zhang, C. Li, C. Tu, H. Zhang, M. Niu, Y. Xiong, X. Xiao, K. Zhao, W. Gao, J.B. Wang, Poria attenuates idiosyncratic liver injury induced by polygoni multiflori radix praeparata, Front. Pharmacol. 7 (2016) 386.
[49] L. Lin, H. Lin, M. Zhang, B. Ni, X. Yin, C. Qu, J. Ni, A novel method to analyze hepatotoxic components in polygonum multiflorum using ultra-performance liquid chromatography-quadrupole time-of-flight mass spectrometry, J. Hazard. Mater. 299 (2015) 249–259.
[50] J. Yu, J. Xie, X. Mao, M. Wang, N. Li, J. Wang, G. Zhaori, R. Zhao, Hepatoxicity of major constituents and extractions of radix polygoni multiflori and radix polygoni multiflori praeparata, J. Ethnopharmacol. 137 (2011) 1291–1299.
[51] Y. Wu, S. Huang, J. Wang, L. Sun, F. Zeng, S. Wu, Activatable probes for diagnosing and positioning liver injury and metastatic tumors by multispectral optoacoustic tomography, Nat. Commun. 9 (2018) 3983.
[52] Y. Huang, H. Chern, W. Su, J. Wu, S. Chang, C. Chiang, F. Chang, S. Lee, Cytochrome P450 2E1 genotype and the susceptibility to antituberculosis drug-induced hepatitis, Hepatology 37 (2003) 924–930.
[53] U.A. Boelsterli, K.K. Lee, J. Gastroenterol, Mechanisms of isoniazid-induced idiosyncratic liver injury: emerging role of mitochondrial stress, Hepatology 29 (2014) 678–687.
[54] D.S. Dickinson, W.C. Bailey, B.I. Hirschowitz, S.J. Soong, L. Eidus, M.M. Hodgkin, Risk factors for isoniazid (NIH)-induced liver dysfunction, J. Clin. Gastroenterol. 3 (1981) 271–279.
[55] I.G. Metushi, T. Nakagawa, J. Uetrecht, Direct oxidation and covalent binding of isoniazid to rodent liver and human hepatic microsomes: humans are more like mice than rats, Chem. Res. Toxicol. 25 (2012) 2567–2576.
[56] I.G. Metushi, P. Cai, X. Zhu, T. Nakagawa, J.P. Uetrecht, A fresh look at the mechanism of isoniazid-induced hepatotoxicity, Clin. Pharmacol. Ther. 89 (2011) 911–914.
[57] C.J. Reinhardt, E.Y. Zhou, M.D. Jorgensen, G. Partipilo, J. Chan, A Ratiometric Acoustogenic Probe for in Vivo Imaging of Endogenous Nitric Oxide, J. Am. Chem. Soc. 140 (2018) 1011–1018.
[58] C. Yin, X. Zhen, Q. Fan, W. Huang, K.Y. Pu, Degradable Semiconducting Oligomer Amphiphile for Ratiometric Photoacoustic Imaging of Hypochlorite, ACS Nano 11 (2017) 4174–4182.

[59] K.Y. Pu, A.J. Shuhendler, J.V. Jokerst, J. Mei, S.S. Gambhir, Z. Bao, J.H. Rao, Semiconducting polymer nanoparticles as photoacoustic molecular imaging probes in living mice, Nat. Nanotech. 9 (2014) 233–239.
[60] Q. Chen, X. Liu, J. Chen, J. Zeng, Z. Cheng, Z. Liu, A self-assembled albumin-based nanoprobe for in vivo ratiometric photoacoustic pH imaging, Adv. Mater. 27 (2015) 6820–6827.
[61] C. Yin, X. Zhen, Q. Fan, W. Huang, K. Pu, Degradable semiconducting oligomer amphiphile for ratiometric photoacoustic imaging of hypochlorite, ACS Nano 11 (2017) 4174–4182.
[62] Y. Liu, S. Wang, Y. Ma, J. Lin, H. Wang, Y. Gu, X. Chen, P. Huang, Ratiometric photoacoustic molecular imaging for methylmercury detection in living subjects, Adv. Mater. 29 (2017) 1606129.
[63] J. Weber, P.C. Beard, S.E. Bohndiek, Contrast agents for molecular photoacoustic imaging, Nat. Methods 13 (2016) 639–650.
[64] A.B. Nair, S. Jacob, A simple practice guide for dose conversion between animals and human, J. Basic Clin. Pharm. 7 (2016) 27–31.
[65] O.L. Blanchard, J.M. Smoliga, Translating dosages from animal models to human clinical trials-revisiting body surface area scaling, FASEB J. 29 (2015) 1629–1634.
[66] C.F. Nagy, J. Mondick, N. Serbina, L.S. Casey, S.E. Carpenter, J. French, R. Guttendorf, Animal-to-human dose translation of obiltoxaximab for treatment of inhalational anthrax under the US FDA animal rule, Clin. Transl. Sci. 10 (2017) 12–19.
[67] J. Ma, L. Zheng, Y.S. He, H.J. Li, Hepatotoxic assessment of Polygoni Multiflori Radix extract and toxicokinetic study of stilbene glucoside and anthraquinones in rats, J. Ethnopharmacol. 162 (2015) 61–68.
[68] X. Wu, X. Chen, Q. Huang, D. Fang, G. Li, G. Zhang, Toxicity of raw and processed roots of polygonum multiflorum, Fitoterapia 83 (2012) 469–475.
[69] Q. Dong, N. Li, Q. Li, C. Zhang, W. Feng, G. Li, R. Li, C. Tu, X. Han, Z. Bai, Y. Zhang, M. Niu, Z. Ma, X. Xiao, J. Wang, Screening for biomarkers of liver injury induced by polygonum multiflorum: a targeted metabolomic study, Front. Pharmacol. 6 (2015) 217.

Yinglong Wu Dr. Yinglong Wu received his BASc degree from South China University of Technology in 2014, and then he pursued the PhD degree in materials science at South China University of Technology under the supervision of Prof. Shuizhu Wu. He submitted his doctoral thesis to College of Materials Science & Engineering - South China University of Technology in 2018. His research interests include materials synthesis and optoacoustic and fluorescent sensing.

Lihe Sun Lihe Sun received the BASc degree from South China University of Technology in 2017. He is currently pursuing the PhD degree in materials science at South China University of Technology under the supervision of Prof. Shuizhu Wu. His research interests include materials synthesis, optoacoustic and fluorescent detection.

Fang Zeng Fang Zeng has been a professor at the College of Materials Science and Engineering, South China University of Technology, Guangzhou, China since 2004. His primary research interests include chromophore materials, nanoparticles, chemosensors and biosensors, and drug delivery systems.

Shuizhu Wu Shuizhu Wu has been a professor at State Key Laboratory of Luminescent Materials and Devices, College of Materials Science and Engineering, South China University of Technology, Guangzhou, China since 2005. Her primary research interests include chromophore materials, photophysics, chemosensors and biosensors, nanoparticles, and biomaterials.